# Correlation between reflectance indices and the electrical conductivity of the soil in the Lajas Valley, Puerto Rico

José Pablo Castro-Chacón - jose.castro23@upr.edu
Department of Agro-environmental Sciences, University of Puerto Rico - Mayaguez Campus.

## Abstract

The apparent electrical conductivity of the soil (ECa) was measured in three pilot plots located in the Lajas Valley using an EM-38, and electromagnetic induction sensor (EMI). The ECa signal was correlated with multispectral images of the Landsat 8 and Sentinel 2A using different vegetation and salinity indexes. A digital elevation model (DEM) from a LIDAR sensor was considered to evaluate and understand how the ECa signal is related with the relieve. The preliminary results show a statistically significant relationship between the ECa spatial distribution and the different indexes of the remote sensors evaluated. This study concluded the viability of combine the use of ECa and multispectral images for the digital mapping of saline and sodic soils in the Lajas Valley Agricultural Reserve (LVAR).

**Keywords** *electromagnetic induction, ECa, EM-38, Lajas Valley, Landsat 8, Sentinel 2, LIDAR, soils*

## Introduction

Digital soil mapping has incorporated the use of modern techniques as electromagnetic induction (EMI) and remote sensing (RS) to create thematic edaphological maps that represents the spatial and temporal distribution of soil parameters. The EMI technique incorporates a soil electrical conductivity meter (EM-38) to receive the apparent electrical conductivity (ECa). This signal is used to infer physical and chemical soil properties, while different global satellites allow us to obtain accurate information of the earth surface at different spatial, temporal, radiometric and spectral scales. Through the combination of both technologies is possible to create regional maps to predict soils and environmental conditions, such as saline and sodic toxicity, which are recurrent in the Lajas Valley.

Bonnet and Brenes (1958) studied the problems of salinity and sodicity of the soil in the Valley of Lajas using a grid of soil samples, they determined that in a depth of 0 to 60 cm the saline, saline-sodic and sodic lands were 9,700 ha. The origin of the salts in the Valley of Lajas is associated with the geological formation process, since it is recognized that this territory was under direct influence of the sea, which would have led to a large accumulation of these minerals within the stratigraphic column. Coupled with this, the climatic conditions characteristic of a semi-arid regime increase the salinity problems, since these salts accumulated in the soil profiles do not dissolve easily, if don’t they are exposed on the surface and affect the root zone of the plants, decreasing the productivity of the crops and causing the mortality of the plants. There are also other problems of associated anthropogenic origin such as excessive irrigation with high salt concentrations.

Since 1980, with the appearance of the first electromagnetic induction instruments, there has been a considerable increase in the number of investigations carried out on the cartography of sodicity and salinity soils, Cameroni et al. (1980) made in Canada (a country that was a pioneer in the development of this type of equipment, with the Geonics company that still operates today) a correlation between the ECa signal captured by the EM38 instrument and the results obtained from a soil analyst of effective electric conductivity (ECe) in samples of saturated paste soil and determined that there was a high correlation between both variables. Similar studies with the same techniques were carried out in the United States by members of the US Salinity Lab, such as the works of Wollenhaupt et al. (1986) and Rhoades et al. (1989).

In the decade of 1990 the works of mapping of salinity and sodicity of soils increase considerably, the first advances in the use of remote sensors are given as a technique of regional cartography, most of the investigations continue to correlate the induction electromagnetic with soil chemical analysis. The first identified works that make use of remote sensors were those of Mougenot, Pouget and Epema (1993) developed in France, Verma et al. (1994) employed in India, Wiegand et al. (1994) in the United States and Eklund (1998) in Australia.

Since 2000, studies using RS with EMI are numerous, in many parts of the world this technology is being applied to predict the distribution of saline soils. It's important to mention the investigations carried out by the United States Salinity Lab team, Scudiero, Skaggs y Corwin (2014), Scudiero, Skaggs y Corwin (2015), Scudiero, Skaggs y Corwin (2016), who executed this procedure to characterize the saline soils of the San Joaquin Valley in California.

**Materials**

- Soil electrical conductivity meter (EM38).
- Multispectral image of the Landsat 8 mission of December 9, 2018, with a percentage of cloudiness of 0%.
- Multispectral image of the Sentinel 2 mission of January 8, 2019, with a percentage of cloudiness of 0%.
- Digital Elevation Model of LIDAR.
- Spectroradiometer GER 1500.

**Remote sensors description**

- Soil electrical conductivity meter (EM38):

The instrument sends an electromagnetic pulse that interacts with the ground and receives the response pulse. This electromagnetic pulse response depends of the mineralogical properties of the soil and it is known as apparent electrical conductivity ECA.

Figure N1. Soil electrical conductivity meter EM38.

- Landsat 8 and Sentinel 2:

They are sensors that have some similar characteristics but also big differences. The blue, green and red bands on both sensors are practically the same. Landsat 8 has a panchromatic band, whereas Sentinel 2 does not have, however Sentinel 2 has a better spatial resolution than Landsat 8, so this panchromatic band is not as important.

Sentinel 2 has four bands in the near infrared which allows it to capture greater differences in the vegetation, while Landsat 8 only has one. Sentinel 2 has a band to detect water vapor while Landsat 8 does not specifically. With respect to the medium infrared bands are very similar, each sensor has three. Finally, Landsat 8 has thermal sensors whereas Sentinel 2 does not have. Below is a table with the differences.

Table N1. Technical characteristics of Landsat 8 and Sentinel 2.

| Landsat 8 OLI & TIRS Multispectral Image | | | Sentinel 2A Multispectral Image | | |
|---|---|---|---|---|---|
| Bands | Central Wavelenght (nm) | Resolution (m) | Bands | Central Wavelenght (nm) | Resolution (m) |
| B1 Coastal | 440 | 30 | B1 Coastal | 443 | 60 |
| B2 Blue | 480 | 30 | B2 Blue | 490 | 10 |
| B3 Green | 560 | 30 | B3 Green | 560 | 10 |
| B4 Red | 650 | 30 | B4 Red | 665 | 10 |
| B8 Panchomatric | 590 | 15 | | | |
| | | | B5 NIR | 705 | 20 |
| | | | B6 NIR | 740 | 20 |
| | | | B7 NIR | 783 | 20 |
| B5 NIR | 865 | 30 | B8A NIR | 865 | 20 |
| | | | B9 Water vapour | 945 | 60 |
| B9 SWIR Cirrus | 1370 | 30 | B10 SWIR Cirrus | 1375 | 60 |
| B6 SWIR | 1610 | 30 | B11 SWIR | 1610 | 20 |
| B7 SWIR | 2200 | 30 | B12 SWIR | 2190 | 20 |
| B10 Thermal | 10895 | 100 | | | |
| B11 Thermal | 12005 | 100 | | | |

- LIDAR sensor:

A high resolution digital elevation model obtained with a LIDAR sensor was used, it was obtained from the USGS electronic database and was captured in 2016.

- Spectroradiometer GER 1500:

This instrument was used to measure the reflectance of certain objects in the field, to understand what are the differences between different soil coverings and the internal differences between each surface.

**Methods**

**A. Capture the ECa signal:**

The ECa signal was measured in three plots of the Lajas Valley, this measurement was calculated in vertical position with penetration of 1.5 meters. The total area sampled corresponds to 18 hectares, was selected arbitrarily with the intention of conducting preliminary studies on two soil series, Fe and Guánica, which have been identified by NRCS with salinity problems.

Figure N2. Study Plots

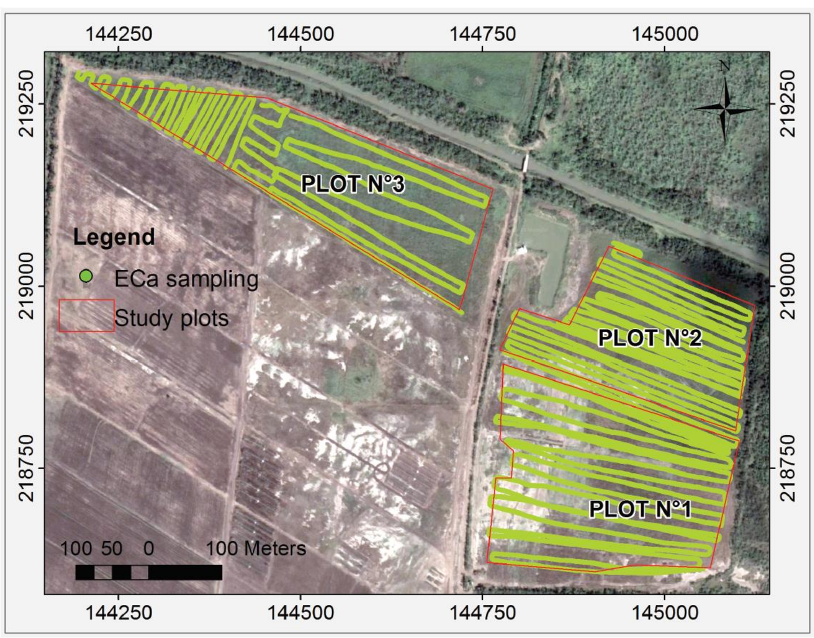

### B. Interpolation of the ECa:

The ECa signal was interpolated by means of the ordinary kriging method, which is recommended for high density point clouds like the one used in this case. Remember that the EM38 captures ten data per second. The ECa maps were created in a 30x30 pixel size to be able to correlate these on a regional scale with the sensors of Landsat 8 and Sentinel 2.

Figure N3. ECa signal in vertical position

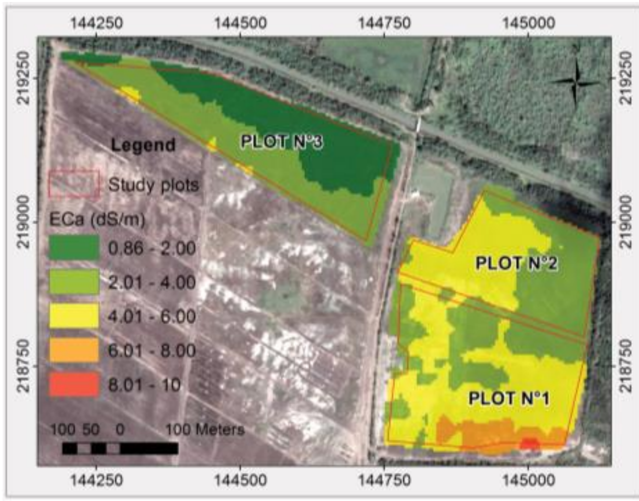


### C. Landsat 8 and Sentinel 2A indices:

From the multispectral images a series of indices were calculated, which were recommended by different authors reviewed in the literature.

Table N2. Calculated Indices of Landsat 8 and Sentinel 2.

| | | |
|---|---|---|
| **NDVI** | $\frac{\text{NIR}-\text{RED}}{\text{NIR}+\text{RED}}$ | Asfaw et al. (2016) |
| **SAVI** | $\frac{800\text{nm}-670\text{nm}}{800\text{nm}+670\text{nm}+L}(1+L)$ | Asfaw et al. (2016) |
| **DVI** | **NIR-RED** | From: indexdatabase.de |
| **CRSI** | $\sqrt{\frac{NIRxRED-GxB}{NIRxRED+GxB}}$ | Scudiero et al. (2014) |
| **NDVI2** | $\frac{\text{MIR}-\text{NIR}}{\text{MIR}+\text{NIR}}$ | From: indexdatabase.de |
| **NDSI=** | $NDSI=\frac{(R-NIR)}{(R+NIR)}$ | Azabdaftari, A, y Sunarb, F. (2016) |
| **SI** | $\sqrt{\text{B1}*\text{B3}}$ | Gorija et al. (2017) |
| **SI3** | $\sqrt{(\text{B2})^2+(\text{B3})^2+(\text{B4})^2}$ | Gorija et al. (2017) |
| **SI9** | $\frac{(B_5\times B_6-B_6\times B_6)}{B_5}$ | Azabdaftari, A, y Sunarb, F. (2016) |
| **VSSI** | **2 x B2 – 5 x (B3+B4)** | Asfaw et al. (2016) |
| **Natural Bands** | Each of the individual bands was evaluated as an index | From: indexdatabase.de |

Figure N4. Example of some of the indices calculated with Landsat 8 and S2.

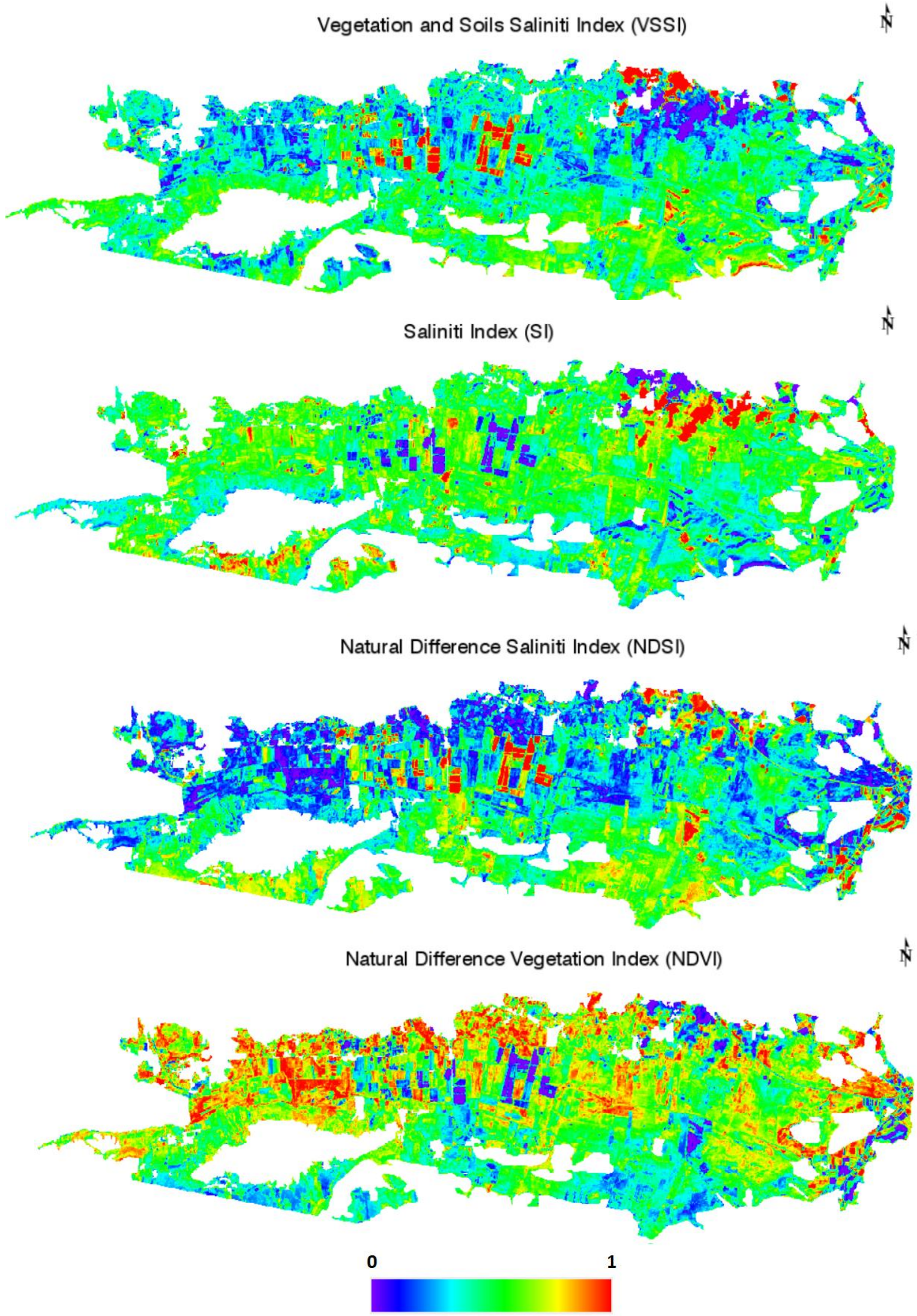

### D. Pearson Correlations:

ECa maps were transferred to central points considering the value of each one pixel. This coverage of points was intersected with each of the Landsat 8 and Sentinel 2A bands and indices to obtain paired data series. With this data, a Pearson correlation model was constructed through the following equations.

$$r = \frac{\theta xy}{\theta x * \theta y} \qquad \theta xy = \frac{\sum_{i=1}(xi - \bar{x})(yi - \bar{y})}{n}$$

Where:

r = Pearson correlation coefficient

θxy = Covariance

θ = Standard deviation

x = Observed variable (Multispectral bands)

y = Inferred variable (ECa)

n = Number of data

**Results**

**Plot N1:** This land was planted with natural grass at the time of measurement, the table N3 shows the bands and indices with results higher than 0.6 in the Pearson R.

Table N3. Correlation between ECa and multispectral bands (Plot 1)

| SENSOR | R PEARSON | ECA_V_UTM |
|---|---|---|
| LANDSAT 8 | OLI NDVI2 | -0.68 |
| LANDSAT 8 | OLI NDVI | -0.68 |
| LANDSAT 8 | OLI SAVI | -0.68 |
| SENTINEL 2 | B05 | 0.61 |
| SENTINEL 2 | B12 | 0.61 |
| LANDSAT 8 | OLI SI9 | 0.61 |
| SENTINEL 2 | SENTINEL SI | 0.62 |
| LANDSAT 8 | B3 | 0.66 |
| LANDSAT 8 | B4 | 0.66 |
| LANDSAT 8 | B1 | 0.68 |
| LANDSAT 8 | B2 | 0.68 |
| LANDSAT 8 | OLI NDSI | 0.68 |
| LANDSAT 8 | OLI SI | 0.70 |
| SENTINEL 2 | B04 | 0.73 |
| SENTINEL 2 | B02 | 0.75 |
| LANDSAT 8 | B8 | 0.77 |
| LANDSAT 8 | OLI SI2 | 0.78 |
| LANDSAT 8 | OLI SI3 | 0.78 |
| SENTINEL 2 | B03 | 0.78 |

The results show that both, the Landsat 8 sensor and Sentinel 2 can to strongly predict the ECa signal in that case. The best prediction for L8 was panchromatic band and the best index was Salinity 3. While for Sentinel 2 the best prediction was obtained in band 3 and in the index Salinity 1. In that case LIDAR DEM is not a good predictor.

The following graphic is a linear regression model using the best predictive band, in this case the green band of Sentinel 2.

Graphic N°1. Linear regression between ECa and Band 3 (S2 – Plot 1)

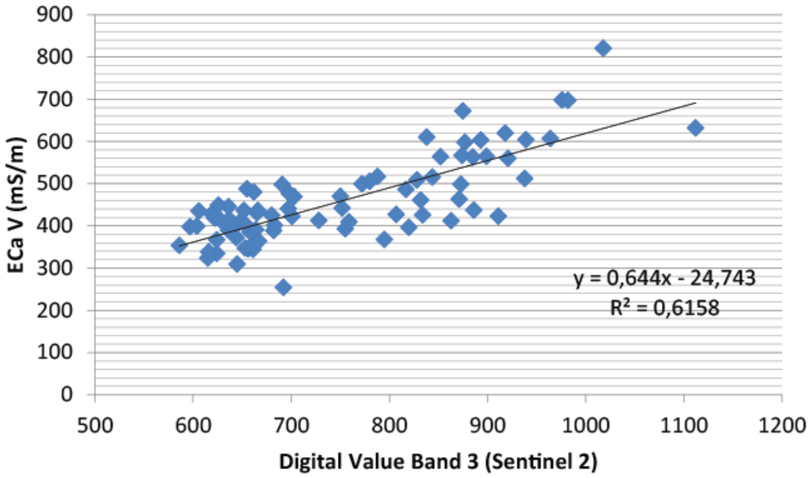


The results show a direct relation and a $R^2$ of 0.61 which indicates that it is a good band to predict ECa to regional scales.

**Plot N2:** This land was plow at the time of measurement, the table N4 shows the bands and indices with results higher than 0.6 in the Pearson R.

Table N4. Correlation between ECa and multispectral bands (Plot 2)

| SENSOR | R PEARSON | ECA_V_UT |
|---|---|---|
| LANDSAT 8 | B5 | -0.76 |
| LANDSAT 8 | B6 | -0.71 |
| LANDSAT 8 | B3 | -0.69 |
| LANDSAT 8 | OLI SI9 | -0.68 |
| LANDSAT 8 | OLI SI | -0.67 |
| LANDSAT 8 | B8 | -0.66 |
| LANDSAT 8 | OLI DVI | -0.64 |
| SENTINEL 2 | B11 | -0.63 |
| SENTINEL 2 | B08 | -0.63 |
| SENTINEL 2 | B07 | -0.62 |
| SENTINEL 2 | B03 | -0.62 |
| SENTINEL 2 | B06 | -0.62 |
| SENTINEL 2 | B05 | -0.61 |
| LANDSAT 8 | OLI SAVI | -0.60 |
| LANDSAT 8 | OLI NDVI2 | -0.60 |
| LANDSAT 8 | OLI NDVI | -0.60 |
| LANDSAT 8 | OLI NDSI | 0.60 |
| LIDAR | DEM | 0.61 |
| LANDSAT 8 | OLI VSSI | 0.68 |

The results show that both, the Landsat 8 sensor and Sentinel 2 can to strongly predict the ECa signal in that case. The best prediction for L8 was the infrared band and the best index was Salinity 9 and VSSI.

While for Sentinel 2 the best prediction was also obtained in band infrared. In that case LIDAR DEM is a good predictor, so the elevation is related to salinity.

The following graphic is a linear regression model using the best predictive band, in this case the infrared band of Landsat 8.

Graphic N°2. Linear regression between ECa and Band 5 (L8) (Plot 2)

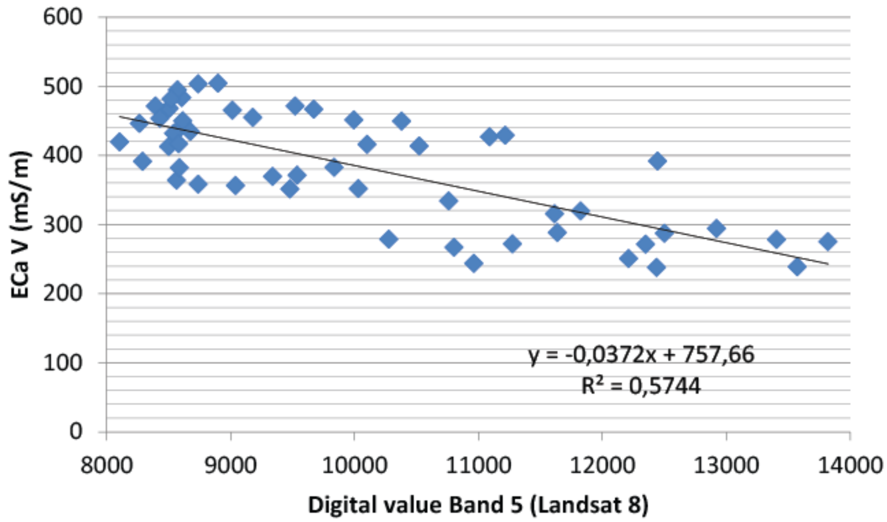


The results show a inverse relation and a $R^2$ of 0.57 which indicates that it is a good band to predict ECa to regional scales.

**Plot N3:** This land was planted with natural grass at the time of measurement, the table N5 shows the bands and indices with results higher than 0.6 in the Pearson R.

Table N5. Correlation between ECa and multispectral bands (Plot 3)

| SENSOR | R PEARSON | ECA_V_UT |
|---|---|---|
| SENTINEL 2 | B09 | -0.88 |
| LANDSAT 8 | B7 | -0.71 |
| LANDSAT 8 | B6 | -0.71 |
| SENTINEL 2 | B01 | -0.67 |
| LIDAR | DEM | 0.78 |

The results show that both, the Landsat 8 sensor and Sentinel 2 can to strongly predict the ECa signal, but there were few bands and indices with good results with respect to those obtained in plots 1 and 2. The best prediction for L8 was the mid infrared. While for Sentinel 2 the best prediction was tha band of water vapour. In that case LIDAR DEM is a good predictor, so the elevation is related to salinity.

The following graphic is a linear regression model using the best predictive band, in this case the water vapour band of Sentinel 2.

Graphic N°3. Linear regression between ECa and Band 9 (S2) (Plot 3)

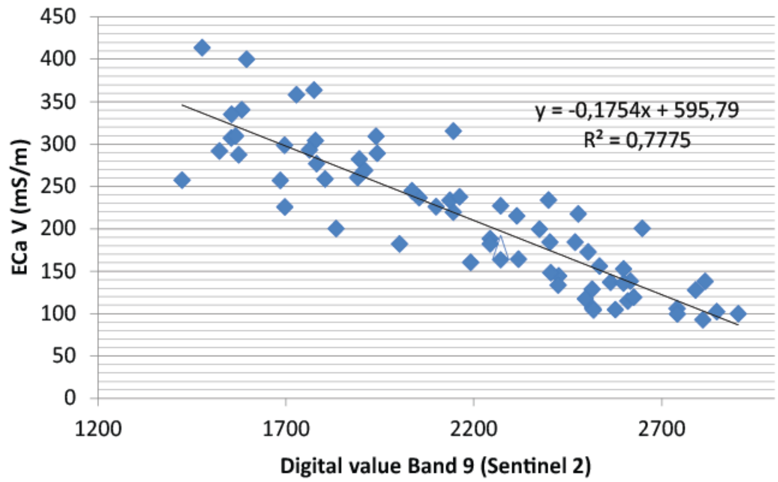


The results show a inverse relation and a $R^2$ of 0.77 which indicates that it is a good band to predict ECa to regional scales.

**Discussion of results**

For plot No. 1, the statistical assessment determined that the band with the highest correlation was the B3 (Green) of the Sentinel A2 sensor, with a Pearson r of 0.78. It was possible to construct a graph of B3 with the ECa to make a linear regression model, it was determined that using the formula y=0.664x-24.743 it is possible to obtain a good prediction of ECa with an $R^2$ equal to 0.61. For plot No. 2, was possible to construct a graph of B5 (Infrared) of the Landsat 8 sensor with the ECa to make a linear regression model, it was determined that using the formula y=0.372x+757.66 it is possible to obtain a good prediction with an $R^2$ equal to 0.57. For plot No. 3, the band with the highest correlation was the B9 (Water Vapour) of the Sentinel 2 sensor, with a Pearson r of -0.88. It was possible to construct a graph of B9 with the ECa to make a linear regression model, it was determined that using the formula y=-0.1754x+595.79 it is possible to obtain a good prediction with an $R^2$ equal to 0.77.

For each one of the properties, good correlations were obtained between the ECa and the bands and spectral indices, this means that it is possible to generate prediction models of these variables. Now it was observed that the best predictions vary, this means that the best bands are not the same for plot 1, 2 or 3, since they have different characteristics. These characteristics are related to soil cover, texture, mineralogical properties, elevation and position in the landscape.

This means that to generate a prediction of ECa for the entire Lajas Valley, these auxiliary quantitative and qualitative variables must be integrated into a multivariable statistical model, to minimize spatial differences. These special differences are because different land coverings have different reflectance patterns therefore, it is not possible to predict the ECA signal with only one equation. Figure N5 and graph N4 show how different surfaces have different reflectance curves.

Figure N5. Different reflectance surfaces were measured with the spectroradiometer GER1500.

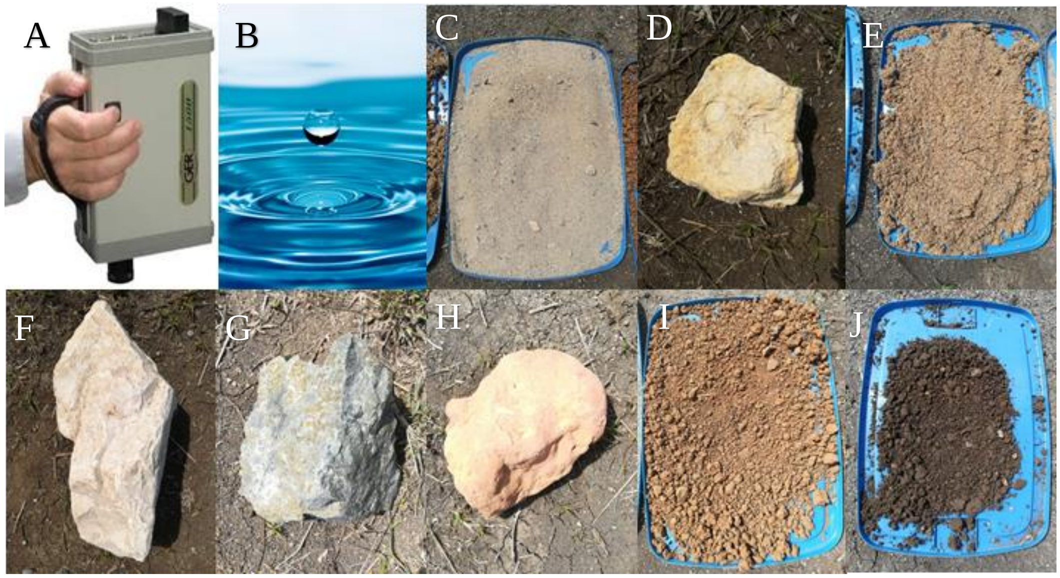


Picture A - Spectroradiometer GER1500. Picture B - Water. Picture C – Dry sand. Picture D – Limestone. Picture E – Wet sand. Picture F – White rock. Picture G – Serpentine. Picture H – Red Rock. Picture I – Ultisol. Picture J – Vertisol.

Graphic N°4. Reflectance differences in some surfaces.

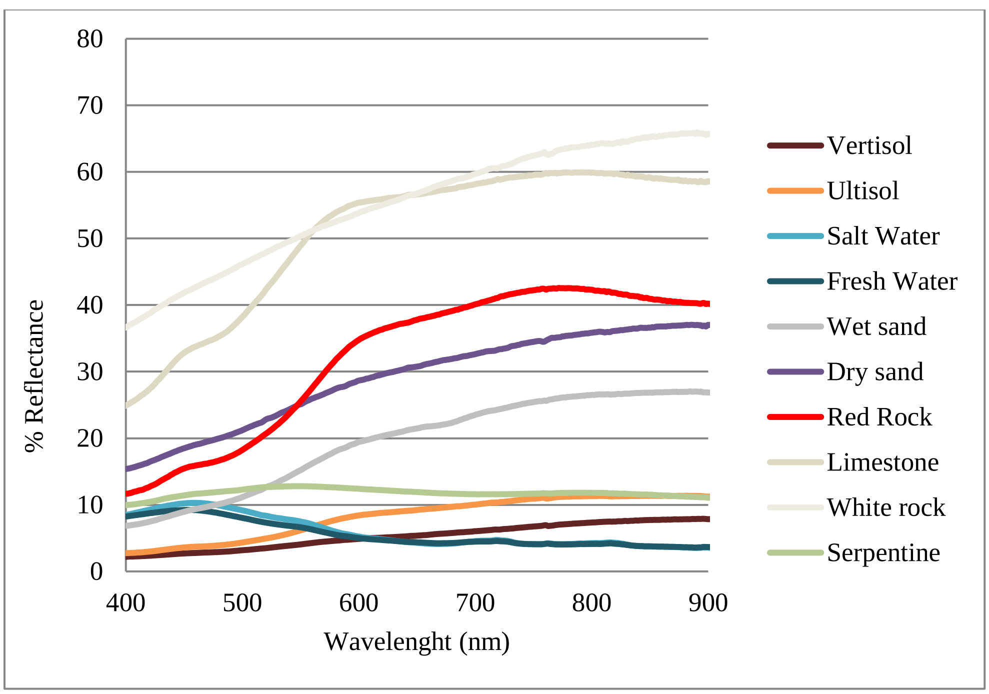

Now each one of these land covers has differences in internal patterns. For example, it is possible to observe more green and leafy pastures in places where the soil has good nutritional content, while we will find yellow pastures in areas where there are problems of toxicity or absence of minerals to supply the needs of the plant.

This experiment could be verified in the soccer field of the University Campus of Mayaguez, where the reflectance of the grass in different sites was measured, obtaining different spectral curves with the same tendency but different intensity.

Graphic N°5. Reflectance differences in pasture surface.

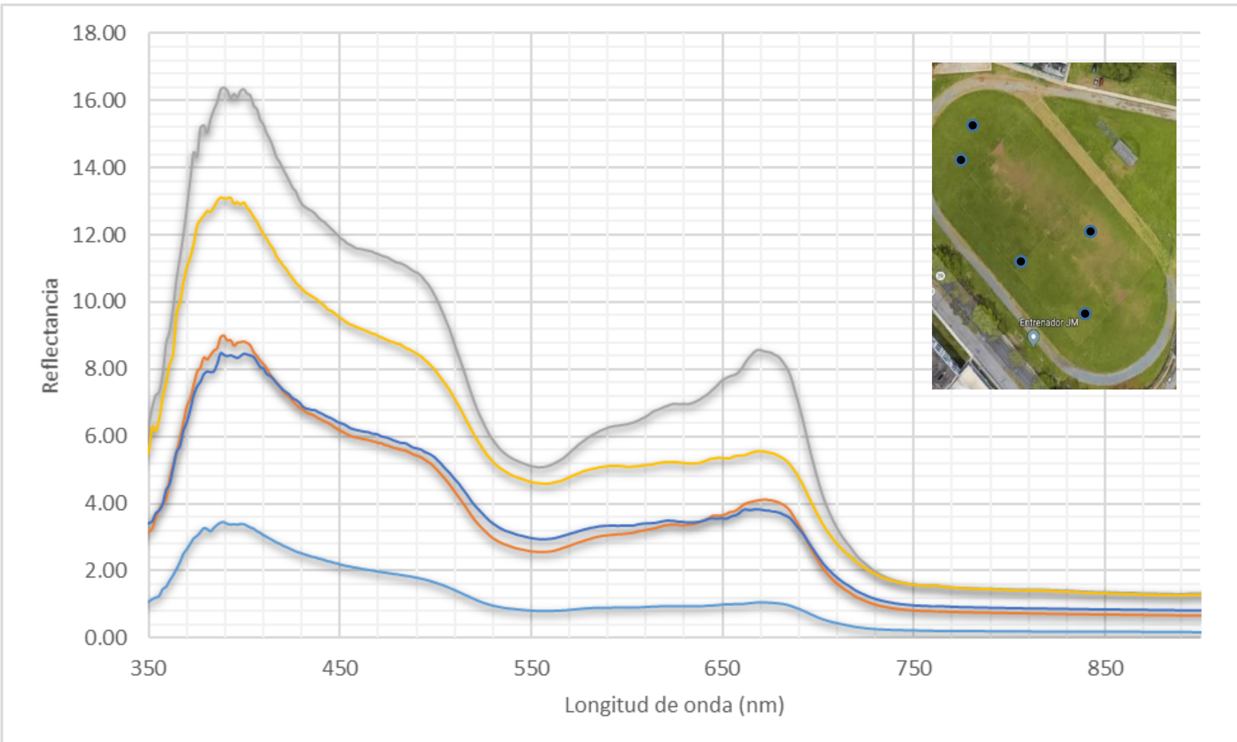


As can be seen in the graph although the measurements are made in a specific use as the grass, there are differences in the intensity of the signal. This internal difference is possible to relate to nutritional or moisture aspects for example.

**Conclusions**

This research demonstrates that it is possible to correlate the ECa signal with multispectral images of Sentinel 2 and Landsat 8 to predict edaphological parameters such as salinity. It is necessary to create differentiated equations considering aspects such as terrain coverage, elevation and texture, this in order to eliminate errors due to variability between different terrain coverings and the internal variability that exists within each one.

Over the next two semesters, ECa data and soil samples will be captured by different lands in the Lajas Valley, with the objective of feeding the predictive model with quality data to create a salinity and sodicity map at a regional scale.

**Aknowledgments**

This project is made possible through the support of the United States Department of Agriculture (USDA), National Institute of Food and Agriculture (NIFA), Hispanic Serving Institution Grant Program (HSI), Award No. 2016-38422-25542. Thanks to Dr. Fernando Gilbes, professor of Remote Sensing Class, also the farm staff for the help and tools provided during the survey.

**Literature cited**

Asfaw, E. et al, (2016) Soil Salinity Modeling And Mapping Using Remote Sensing And Gis: The Case Of Wonji Sugar Cane Irrigation Farm, Ethiopia Journal Of The Saudi Society Of Agricultural Sciences (2018) 17, 250–258

Azabdaftari, A, y Sunarb, F. (2016) Soil Salinity Mapping Using Multitemporal Landsat Data The International Archives Of The Photogrammetry, Remote Sensing And Spatial Information Sciences, Volume Xli-B7, 2016 Xxiii Isprs Congress, 12–19 July 2016, Prague, Czech Republic

Bonnet, J. y Brenes, B. (1958) Estudio Detallado Sobre Salinidad En El Valle De Lajas Boletin 141 De La EEARP.

Cameroni, D. et al. (1980) Mapping Salinity Using Resistivity And Electromagnetic Inductive Techniques Can. J. Soil Sci. 6l: 61-78.

Eklund, P. (1998) Data Mining And Soil Salinity Analysis International Journal Of Geographical Information Science, 12:3, 247-268

Gorjia, T. et al. (2017) Monitoring Soil Salinity Via Remote Sensing Technology Under Datascarce Conditions: A Case Study From Turkey Ecological Indicators 74 (2017) 384–391

Mougenot, B.  Pouget, M. & Epema, G. (1993) Remote Sensing Of Salt Affected Soils Remote Sensing Reviews, 7:3-4, 241-259

Rhoades, J. et al. (1989) Estimating Soil Salinity From Saturated Soil-Paste Electrical Conductivity Soil Sci. Soc. Am. J. 53:428-433 (1989)

Scudiero, E. et al. (2017) Remote Sensing Is A Viable Tool For Mapping Soil Salinity In Agricultural Lands California Agriculture • Doi: 10.3733/Ca.2017a0009

Scudiero, E. Skaggs, T. y Corwin, D. (2014) Regional Scale Soil Salinity Evaluation Using Landsat 7, Western San Joaquin Valley, California, Usa Geoderma Regional 2–3 (2014) 82–90

Scudiero, E. Skaggs, T. y Corwin, D. (2015) Regional-Scale Soil Salinity Assessment Using Landsat Etm+ Canopy Reflectance Remote Sensing Of Environment 169 (2015) 335–343

Verma, K. et al. (1994) Remote Sensing Technique For Mapping Salt Affected Soils International Journal Of Remote Sensing, 15:9, 1901-1914

Wiegand, C. et al. (1994) Photographic And Videographic Observations For Determining And Mapping The Response Of Cotton To Soil Salinity Remote Sens. Environ. 49:212-223 (1994)

Wollenhaupt, N. et al. (1986) A Rapid Method For Estimating Weighted Soil Salinity From Apparent Soil Electrical Conductivity Measured With An Aboveground Electromagnetic Induction Meter Can. J. Soil Sci. 66: 315-321.